FERROELECTRICS

Scale-free ferroelectricity induced by flat phonon bands in HfO_2

Hyun-Jae Lee[1], Minseong Lee[1], Kyoungjun Lee[2], Jinhyeong Jo[1], Hyemi Yang[1], Yungyeom Kim[1], Seung Chul Chae[2], Umesh Waghmare[3], Jun Hee Lee[1]*

Discovery of robust yet reversibly switchable electric dipoles at reduced dimensions is critical to the advancement of nanoelectronics devices. Energy bands flat in momentum space generate robust localized states that are activated independently of each other. We determined that flat bands exist and induce robust yet independently switchable dipoles that exhibit a distinct ferroelectricity in hafnium dioxide (HfO_2). Flat polar phonon bands in HfO_2 cause extreme localization of electric dipoles within its irreducible half-unit cell widths (~3 angstroms). Contrary to conventional ferroelectrics with spread dipoles, those intrinsically localized dipoles are stable against extrinsic effects such as domain walls, surface exposure, and even miniaturization down to the angstrom scale. Moreover, the subnanometer-scale dipoles are individually switchable without creating any domain-wall energy cost. This offers unexpected opportunities for ultimately dense unit cell–by–unit cell ferroelectric switching devices that are directly integrable into silicon technology.

Ferroelectricity arises from the spontaneous ordering of electric dipoles in a crystal that is reversibly switched to opposite directions under an applied electric field. A ferroelectric oxide, hafnium dioxide (HfO_2), recently emerged as an interesting material because of its robust electric dipoles at nanometer thicknesses and ability to directly integrate into silicon devices (*1*–*3*). The switchability of electric dipoles in HfO_2, a fluorite structure, is expected to be different from that in ABO_3 perovskite-structure oxides (*4*), as hinted by its large coercive field (*5*, *6*) and slow domain propagation (*7*). Unfortunately, the underlying reasons for the stable ferroelectricity and distinct switchability of HfO_2 at an atomic level are poorly understood. The relationship between structure and ferroelectric properties of HfO_2 is crucial for their use in advanced nanoelectronic devices such as nonvolatile memories and low-power logic (*2*).

We show that ferroelectric HfO_2 possesses switchability that is robust even down to irreducible, subnanometer-scale dimensions. This behavior is due to the flat phonon bands intrinsic to the material. Whereas flat bands of electrons, photons, and magnons are known to cause exotic phenomena such as electron lattice (*8*), graphene superconductivity (*9*), and photon (*10*) and magnon localization (*11*), flat bands of polar phonons and their consequences in ferroelectrics are not well understood. The emergence of flat phonon bands in HfO_2 provides a missing link to extend those exotic phenomena to ferroelectrics.

We used first-principles calculations to discover flat bands of polar phonons and consequent localized dipoles, which induce a scale-free ferroelectric order in HfO_2. This order contains a lateral array of vertically aligned polar layers separated by nonpolar spacer layers that are each of half–unit cell width (~2.5 Å). The presence of the spacers in HfO_2 laterally localize the vertical dipoles within its half-unit widths in a steplike manner from one polar layer to the next. Contrary to conventional ferroelectrics, whose spread dipoles fade away below critical nano-dimensions (*4*, *12*–*15*), the localized dipoles, which are stable and switchable down to the subnanometer scale, allow storage of bits in angstrom-size lateral domains without costing any domain-wall formation energy. Vanishingly zero interactions between the ferroelectric dipoles, evidenced by flat bands in HfO_2, explain the unusual phenomena of its large coercive field (*5*, *6*) compared with conventional ferroelectrics (*16*–*21*) and its extremely slow domain propagation (*7*). Because HfO_2 is already integrated into silicon technology, fabrication of ultimately dense memories could be accomplished by exploiting its irreducible unit cell–scale switchability.

To determine the origin of unusual structural features of the orthorhombic phase of HfO_2 ($Pca2_1$), we analyzed the sequence of symmetry-lowering steps starting with the cubic $Fm\bar{3}m$ structure of HfO_2, which is known to be stable above 2870 K (*22*). Upon cooling, it transforms into tetragonal $P4_2/nmc$ phase at 2870 K, and then to monoclinic phase at T = 2000 K. By contrast, the ferroelectric orthorhombic phase is stabilized in thin films at

[1]School of Energy and Chemical Engineering, Ulsan National Institute of Science and Technology (UNIST), Ulsan, 44919, Republic of Korea. [2]Department of Physics Education, Seoul National University, Seoul 08826, Republic of Korea. [3]Theoretical Sciences Unit, Jawaharlal Nehru Centre for Advanced Scientific Research, Jakkur, Bangalore 560064, India. *Corresponding author. Email: junhee@unist.ac.kr

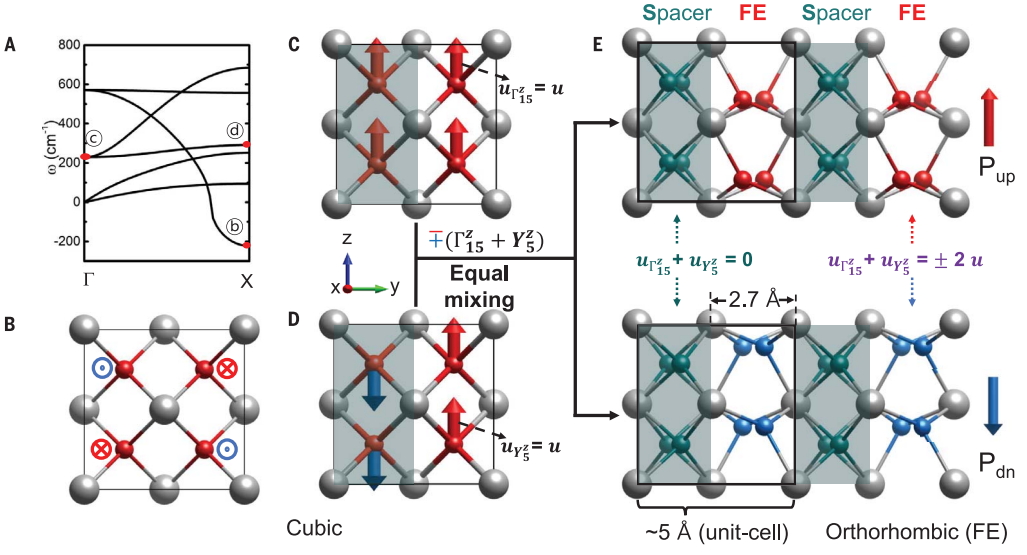

Fig. 1. Structural origin of alternating ferroelectric and nonpolar layers in orthorhombic HfO_2. (**A**) Phonon dispersion of the cubic phase. The red dots labeled b, c, and d denote the primary instability of (**B**) X'_2 mode, (**C**) Γ^z_{15}, and (**D**) Y^z_5, respectively, where arrows denote u, the displacements of oxygen atoms. (**E**) Polar Γ^z_{15} and antipolar Y^z_5 phonons condense in-phase with equal magnitude to generate an orthorhombic structure that consists of alternating spacer layers and ferroelectric layers with up (top), and down (bottom) polarization, respectively. Silver spheres indicate Hf atoms; red and blue spheres indicate oxygen atoms in the ferroelectric layer with up and down polarization, respectively; and green spheres indicate oxygen atoms belonging to the spacer layer.

room temperature (*1*). Phonon spectrum of the high-temperature cubic phase (Fig. 1A) reveals the dominant phonon instability with X'_2 symmetry at $\omega = -i$ 228 cm^{-1}, which involves antiparallel x displacements of neighboring oxygen atoms in the yz plane (Fig. 1B). The cubic structure transforms into a tetragonal structure through the condensation of an X'_2 phonon with zero net polarization. Among the four phonons condensing in the transformation from tetragonal to orthorhombic (fig. S1), we focused on (i) the Γ^z_{15} phonon with all oxygen atoms moving along the z direction (Fig. 1C) generating a uniform polarization and (ii) the cell-doubling antipolar phonon Y^z_5, where oxygen atoms in neighboring xz planes move along the z axis in an antiparallel manner (Fig. 1D), providing A-type ordering with zero net polarization. Similar to strained ZrO_2 (*23*), ferroelectricity of HfO_2 is improperly caused by the nonlinear interaction of stable Γ^z_{15} and X_5 phonons with the primary instability of the X'_2 phonon.

An unusual aspect of the ferroelectric order originates from polar Γ^z_{15} and antipolar Y^z_5 phonons condensing with exactly identical amplitudes, which generate a dipolar partitioning into two types (*24*) of alternating atomically thin layers (Fig. 1E). The first type is the spacer with zero z displacements of oxygen atoms, and the second is the ferroelectric layer with parallel z displacements of its oxygen atoms. Thus, spacers are dead layers that screen the elastic interaction between the ferroelectric active layers. Experimental evidence for these layers can be seen in a study that used transmission electron microscopy and named them as minor and major layers, respectively (*25*). The structural characteristics of the spacer layers is discussed in fig. S2.

Natural dipolar partitioning in orthorhombic HfO_2 has substantial consequences for its polarization domain structure, contrary to that of perovskite ferroelectric $PbTiO_3$. As the local polarization vanishes in the spacer layer even in uniformly polarized HfO_2, it inherently hosts a domain wall of vanishing thickness between oppositely polarized (180°) domains (Fig. 2A). Such a domain wall is essentially strain free (Fig. 2, ε_i, where $i = x$, y, and z; and fig. S3), with little change in the local structure and supporting unsuppressed bulk polarization in its neighborhood. This should lead us to expect a high energy cost of a sharp domain wall in HfO_2 because of the $g|\vec{\nabla} \times \vec{P}|^2$ term. But $g \sim 0$ is evident in its flat band of polar phonons (Fig. 2B and supplementary text S1) and makes a sharp domain wall feasible. This flatness of the polar bands results in a phonon velocity of nearly zero (Fig. 2D). The origin of the flatness is discussed with a spring model in fig. S4. The Γ point phonon in the flat band of the lowest frequency (Fig. 2B, black line) involves atomic displacements of all the modes condensed during cubic-to-orthorhombic transition, and that of higher frequency (Fig. 2B, red line) involves polar and antipolar modes. Physically, the elastic interaction between ferroelectric domains is screened by the spacer layer. With contribution mostly from dipole-dipole interactions, the domain wall energy of HfO_2 is weakly negative (~–18 mJ/m^2) (supplementary text, section 2). By contrast, a domain wall separating the 180° polar domains in $PbTiO_3$ is diffuse, with a width of a few unit cells, and the polarization is suppressed in its neighborhood (Fig. 2C). This difference is because some of the polar atomic displacements are shared between adjacent domains in $PbTiO_3$. The parameter g is sizable, as evident in its dispersed polar phonons (*26*) and a finite phonon velocity in $PbTiO_3$ (Fig. 2D).

We sought to establish the stability and switchability of a polar domain that is half a unit cell wide, sandwiched between the spacers, by simulating reversal of its local polarization (Fig. 3A and fig. S6). The two-dimensional (2D) layer with flipped polarization has a robust stability, with a large energy barrier of 1.34 eV that prevents it from switching back to the uniformly polarized state (Fig. 3B). The switching of polarization in the adjacent layer (Fig. 3B) results in a domain that consists of two ferroelectric layers sandwiching a spacer, following a path with a comparable energy barrier of 1.38 eV. Low dependence of domain wall energy on the width of polar domains reveals weak inter–domain wall interaction, as expected from the flat bands. By contrast, our simulation of a single–unit cell–wide domain in $PbTiO_3$ (Fig. 3C) has substantially reduced polarization at the diffused domain wall, and its marginal stability is evident in its tendency to expand spontaneously (with a small energy barrier of 0.024 eV) to domains of larger width

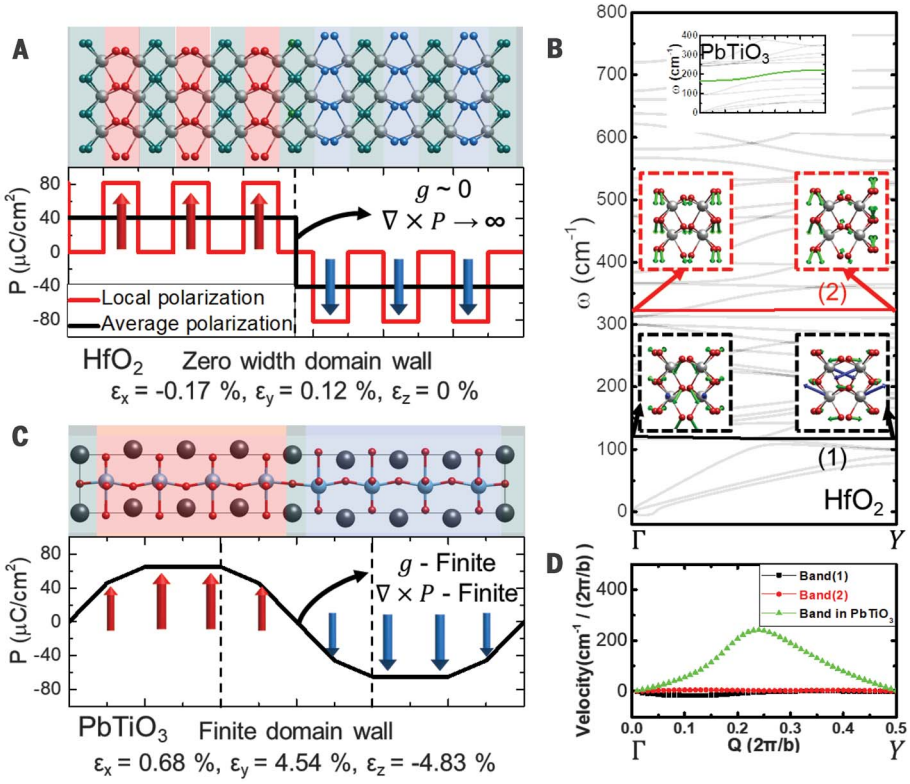

Fig. 2. Flat bands and zero-width domain wall in HfO_2, contrary to the diffused domain wall in $PbTiO_3$. (**A** and **C**) Atomic structure of the domain wall and variation in local polarization along the direction perpendicular to the domain walls in (A) HfO_2 and (C) $PbTiO_3$. Red and black lines correspond to the local polarization averaged over their half– and single–unit cells, respectively. Although ($\vec{\nabla} \times \vec{P} = \frac{\partial P_z}{\partial y}$) is small and spreads over a few unit cells away from the domain wall in $PbTiO_3$, it is singularly large and highly localized at the domain wall in HfO_2. (**B**) This is because of its low energy cost ($g \sim 0$) guaranteed by the flatness of polar phonon bands involving the polar and antipolar modes condensed in orthorhombic HfO_2. Flat polar bands are indicated with black and red lines, and eigenmodes at Γ and Y in the bands are depicted in the insets. This flatness of the bands in HfO_2 is in sharp contrast to a dispersive band in $PbTiO_3$ [(B), top, inset]. (**D**) Phonon velocities of the flat bands in HfO_2 are nearly zero, whereas that of the polar band in $PbTiO_3$ has a finite value. For $PbTiO_3$, black spheres indicate Pb atoms, and light blue and red spheres indicate titanium and oxygen atoms, respectively.

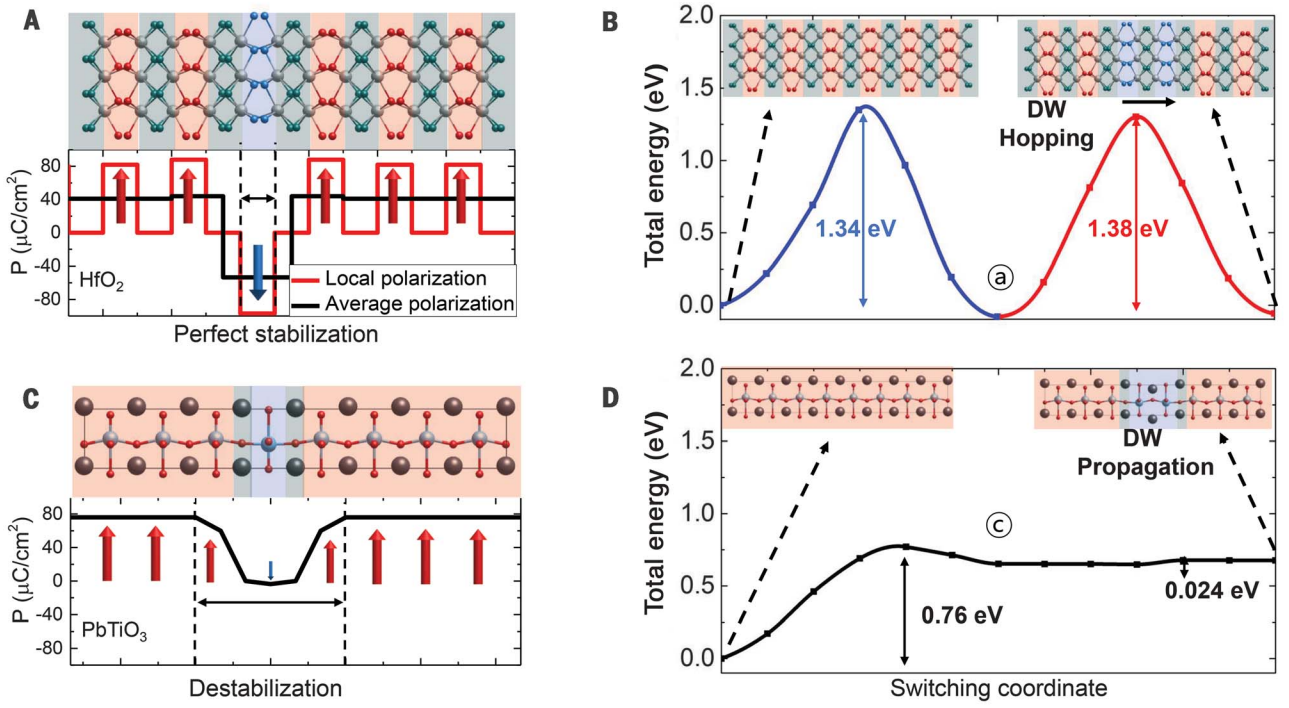

Fig. 3. Robust stability of a half–unit cell–wide ferroelectric domain. (**A**) Atomic structure of the thinnest domain and variation in polarization along the direction perpendicular to the domain walls in HfO_2. (**B**) Energy along the path of polarization switching of HfO_2, starting from the uniformly polarized structure [(B), left inset] to a state with reversed polarization in two layers [(B), right inset] passing through the state in (A). (**C**) In contrast to the domain polarization that is unsuppressed relative to bulk P in HfO_2 (A), it is substantially suppressed inside the switched domain as well as a few unit cells away from the domain wall of $PbTiO_3$. (**D**) The robust stability of a half–unit cell–wide domain of HfO_2 (B) is in complete contrast with the marginal stability of the single–unit cell domain in $PbTiO_3$, which spontaneously expands to wider domains. Successive switching in the next layer [(B), red line] of HfO_2 has an energy barrier comparable with that of the first switching process [(B), blue line] in HfO_2, in contrast to a small energy barrier of successive switching in $PbTiO_3$ (D).

(Fig. 3D). Despite the strongly knit 3D crystal structure of HfO_2, our results establish that it consists of weakly interacting 2D polar layers, allowing stable and switchable ferroelectric domains at the ultimate limit of width (2.7 Å).

We provide a possible explanation of the puzzling observation that the coercive field of polarization switching observed in HfO_2 is unusually large and even comparable with the activation field (E_a). The coercive field (E_c) in conventional ferroelectrics is typically 1/10 of the activation field (Fig. 4A) (*16*) because polarization switching occurs through nucleation and the growth of ferroelectric domains of reversed polarization. Because of such collective behavior, E_c is generally reduced by a factor proportional to the width of the domain wall (*27*). In HfO_2, domain walls are vanishingly thin, and the resulting reduction in E_c (Fig. 4A) is marginal. With weakly interacting domain walls and zero group velocity of the relevant polar modes ($g \sim 0$, by the flat bands of HfO_2), domain walls do not propagate efficiently and can move only by hopping over a large energy barrier (Fig. 3B), suggesting that their sluggish motion observed experimentally could be an intrinsic property (*7*, *28*). By contrast, a domain wall in $PbTiO_3$ encounters a much smaller energy barrier of 0.024 eV (Fig. 3D), and its motion leads to rapid expansion of its polar domain.

We demonstrated the scale-free nature of polarization switching in HfO_2 by comparing reversal of uniform and local polarization (Fig. 4B). Energetics of local and uniform polarization switching in HfO_2 are strikingly similar. Flipping the polarization of a single layer is nearly energetically equivalent (per layer) to flipping the polarization of all layers. By contrast, reversal of local polarization in a single unit cell–wide region is energetically forbidden in $PbTiO_3$. Total energy along the polarization reversal in consecutive 2D polar domains in HfO_2 is a periodic function of the number of unit cell–width domains switched (Fig. 4C). The equal multistability and identical switching barriers show absolutely scale-free behavior that can be labeled by the integer (number of unit cells) and be a basis for a multilevel device whose number of states are similar to the number of lateral unit cells. In contrast to this multistate polar nature in HfO_2, only bistability in $PbTiO_3$ is evident from its uniformly polarized states ($\pm P_0$), which are more stable than the rest of the intermediate polar states (Fig. 4C, bottom).

To establish the intrinsic size limit on ferroelectricity in HfO_2, we simulated Hf-terminated slabs (Fig. 4D) perpendicular to (i) the (010) axis with in-plane polarization and (ii) the (001) axis with out-of-plane polarization. The polarization in a ferroelectric layer of (010) slabs survives in a scale-free manner down to 1.5–unit cell thickness, with spacers acting as natural protective coatings. The polarization retains its bulk value in (001) slabs down to single–unit cell thickness, as expected from the improper nature of fluorite ferroelectricity (*29*). Thus, the intrinsic lateral and perpendicular size limits on ferroelectric order in HfO_2 films are 0.75 and 0.51 nm, respectively (fig. S5). Robust ferroelectric order appears to exist down to 1-nm thickness, as recently reported (*30*), which verifies one of our predictions. Now, the storage size limitation is only from the electrode and the transistor used to interface with it for readout operations.

Because HfO_2 is already compatible in silicon electronics, our discovery of independently switchable polar layers could provide opportunities to realize ultradense and low-cost ferroelectric random-access memory (FeRAM) or a ferroelectric field-effect transistor (FeFET) for memory or logic device applications (figs.

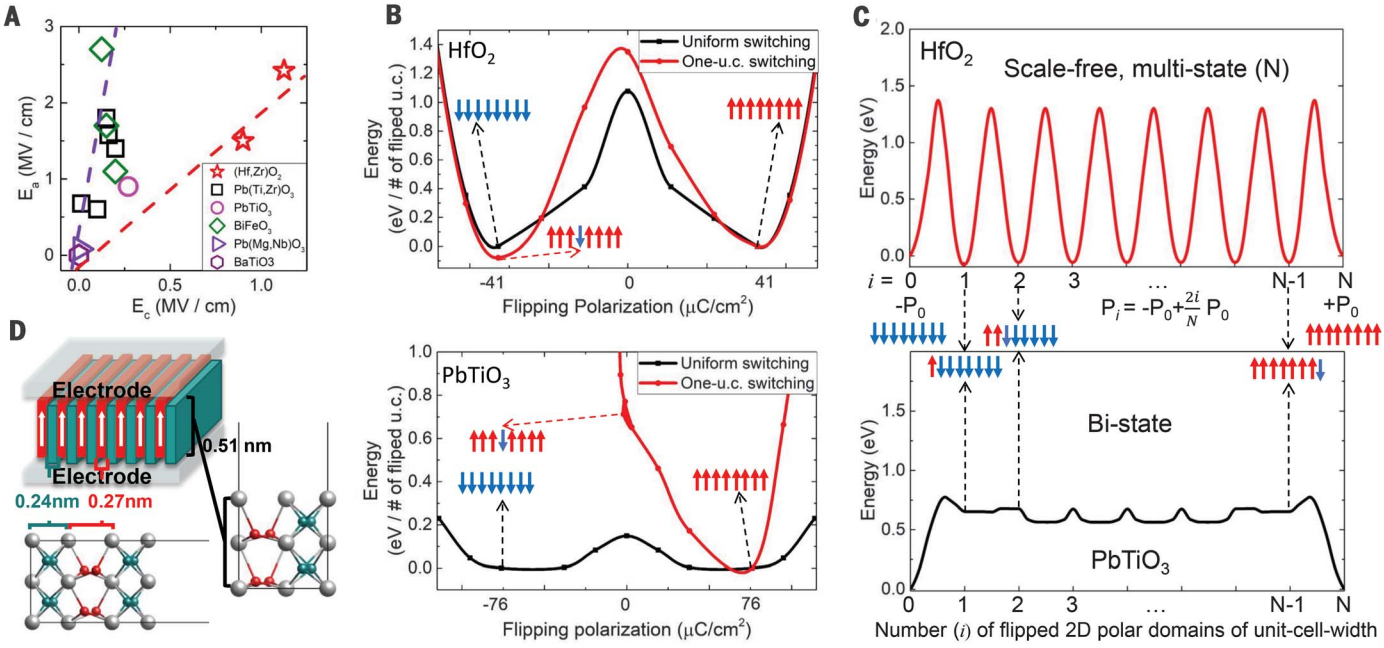

Fig. 4. Experimental activation and coercive fields revealing unusual switching behavior of HfO_2 and simulated energetics demonstrating its fully scale-free 2D domain switching of 0.27-nm width. (**A**) Experimental values of activation (E_a) and coercive (E_c) fields for various ferroelectrics [$BaTiO_3$, (*16*); Pb(Zr,Ti)O_3, (*17*, *18*); $BiFeO_3$, (*19*, *21*); Pb(MgNb)O_3, (*20*); $PbTiO_3$, (*21*); and (Hf,Zr)O_2, (*5*, *6*)]. Although E_c is 10 times smaller than E_a in conventional ferroelectrics, these values are comparable in HZO, implying that collective and individual domain switching occur at the same field. (**B**) Calculated energy curves along paths of switching uniform and local (one unit cell) polarization in HfO_2 (top) and $PbTiO_3$ (bottom). (**C**) Energy of unit cell–by–unit cell width switching. Whereas switching of local polarization in consecutive unit cells in $PbTiO_3$ shows bistable ($\pm P_0$) behavior (bottom), domains of any width in HfO_2 are equally stable with the same energy barrier of switching (top), showing its multistate and scale-free ferroelectric behavior in stability and switchability. (**D**) Schematic of HfO_2-based capacitive memory device with ultrahigh density because the improper ferroelectricity allows no critical thickness, as confirmed with first-principles calculations [(D), right]. There is no critical lateral width of ferroelectricity in HfO_2 [(D), bottom] because of the presence of spacer layers.

S11 and S12). In addition, possibility of unit cell–by–unit cell dipolar control provides different opportunities for deterministic multilevel switching (figs. S6, S7, and S12), ultimately down to the angstrom scale.

REFERENCES AND NOTES

1. T. Böscke, J. Müller, D. Bräuhaus, U. Schröder, U. Böttger, *Appl. Phys. Lett.* **99**, 102903 (2011).
2. T. Mikolajick, S. Slesazeck, M. H. Park, U. Schroeder, *MRS Bull.* **43**, 340–346 (2018).
3. M.-K. Kim, J.-S. Lee, *Nano Lett.* **19**, 2044–2050 (2019).
4. C. H. Ahn, K. M. Rabe, J.-M. Triscone, *Science* **303**, 488–491 (2004).
5. D. Zhou *et al.*, *Acta Mater.* **99**, 240–246 (2015).
6. C. Alessandri, P. Pandey, A. Abusleme, A. Seabaugh, *IEEE Electron Device Lett.* **39**, 1780–1783 (2018).
7. P. Buragohain *et al.*, *Appl. Phys. Lett.* **112**, 222901 (2018).
8. Z. Li *et al.*, *Sci. Adv.* **4**, eaau4511 (2018).
9. Y. Cao *et al.*, *Nature* **556**, 43–50 (2018).
10. S. Mukherjee *et al.*, *Phys. Rev. Lett.* **114**, 245504 (2015).
11. J. Schulenburg, A. Honecker, J. Schnack, J. Richter, H.-J. Schmidt, *Phys. Rev. Lett.* **88**, 167207 (2002).
12. M.-W. Chu *et al.*, *Nat. Mater.* **3**, 87–90 (2004).
13. J. F. Ihlefeld *et al.*, *J. Am. Ceram. Soc.* **99**, 2537–2557 (2016).
14. Y. G. Wang, W. L. Zhong, P. L. Zhang, *Phys. Rev. B Condens. Matter* **51**, 17235–17238 (1995).
15. D. D. Fong *et al.*, *Science* **304**, 1650–1653 (2004).
16. H. Wieder, *J. Appl. Phys.* **28**, 367–369 (1957).
17. V. Nagarajan *et al.*, *J. Appl. Phys.* **86**, 595–602 (1999).
18. J. Son, C. Park, S.-K. Kim, Y.-H. Shin, *J. Appl. Phys.* **104**, 064101 (2008).
19. D. Pantel *et al.*, *J. Appl. Phys.* **107**, 084111 (2010).
20. D. Fu, H. Taniguchi, M. Itoh, S. Mori, Pb($Mg_{1/3}Nb_{2/3}$)O_3 (PMN) Relaxor: Dipole glass or nano-domain ferroelectric?, in *Advances in Ferroelectrics*, vol. 3, A. Peláiz-Barranco, Ed. (IntechOpen, 2012).
21. W.-H. Kim, S. M. Yoon, J. Y. Son, *Mater. Lett.* **124**, 47–49 (2014).
22. R. Terki, G. Bertrand, H. Aourag, C. Coddet, *Mater. Lett.* **62**, 1484–1486 (2008).
23. S. E. Reyes-Lillo, K. F. Garrity, K. M. Rabe, *Phys. Rev. B Condens. Matter Mater. Phys.* **90**, 140103 (2014).
24. R. Materlik, C. Künneth, A. Kersch, *J. Appl. Phys.* **117**, 134109 (2015).
25. E. D. Grimley, T. Schenk, T. Mikolajick, U. Schroeder, J. M. LeBeau, *Adv. Mater. Interfaces* **5**, 1701258 (2018).
26. N. Choudhury, E. J. Walter, A. I. Kolesnikov, C.-K. Loong, *Phys. Rev. B Condens. Matter Mater. Phys.* **77**, 134111 (2008).
27. S. Choudhury *et al.*, *J. Appl. Phys.* **104**, 084107 (2008).
28. H. Mulaosmanovic *et al.*, *ACS Appl. Mater. Interfaces* **9**, 3792–3798 (2017).
29. N. Sai, C. J. Fennie, A. A. Demkov, *Phys. Rev. Lett.* **102**, 107601 (2009).
30. S. S. Cheema *et al.*, *Nature* **580**, 478–482 (2020).

ACKNOWLEDGMENTS

We thank N. Spaldin for critical and constructive comments on the manuscript. J.H.L. appreciates Y. Kim, H. Kang, C. H. Kim, and H.-S. Kim for useful discussions. **Funding:** This work is supported by the Creative Materials Discovery (2017M3D1A1040828), the MOTIE (Ministry of Trade, Industry Energy) (10080657), KRSC (Korea Semiconductor Research Consortium) program, and Basic Research Laboratory (NRF2017R1A4A1015323). U.W. thanks UNIST for hospitality and funding from a J. C. Bose National Fellowship of SERB, Government of India, and support from the Department of Science and Technology for the India-Korea Joint Network Center in computational materials science. We appreciate the Supercomputing Center/Korea Institute of Science and Technology Information for supercomputing resources, including technical support (KSC-2020-CRE-0088). **Author contributions:** J.H.L. conceived the idea and supervised the work. H.-J.L., Y.K., U.W., and J.H.L. designed and carried out density functional theory calculations, and M.L., H.Y., and J.J. helped with analysis of the data. K.L. and S.C.C. provided experimental verifications. J.H.L., U.W., and H.-J.L. developed the theory and wrote the manuscript. **Competing interests:** J.H.L. and H.-J.L. are inventors on KR patent application (10-2020-0047206) submitted by the Ulsan National Institute of Science and Technology (UNIST) that covers ultimately high-density ferroelectric memories and deterministic multilevel devices induced by flat phonon bands. **Data and materials availability:** All data are available in the main text or the supplementary materials.

SUPPLEMENTARY MATERIALS

science.sciencemag.org/content/369/6509/1343/suppl/DC1
Materials and Methods
Supplementary Text S1 to S3
Figs. S1 to S15
References (*31*–*70*)

28 October 2019; resubmitted 29 April 2020
Accepted 16 June 2020
Published online 2 July 2020
10.1126/science.aba0067

Scale-free ferroelectricity induced by flat phonon bands in HfO_2

Hyun-Jae Lee, Minseong Lee, Kyoungjun Lee, Jinhyeong Jo, Hyemi Yang, Yungyeom Kim, Seung Chul Chae, Umesh Waghmare, and Jun Hee Lee

Science **369** (6509), . DOI: 10.1126/science.aba0067

Switching to the atomic scale

Ferroelectric materials are attractive because they provide a way to change electrical resistance by using an electric field. Lee *et al.* used simulations to explain the persistence of ferroelectric behavior in very thin films of hafnium oxide (see the Perspective by Noheda and Íñiguez). The authors' calculations show that ferroelectric properties should be found in films below 1 nanometer thick. This makes the material very attractive for the next generation of random access memory.

Science, this issue p. 1343; see also p. 1300

Science (ISSN 1095-9203) is published by the American Association for the Advancement of Science. 1200 New York Avenue NW, Washington, DC 20005. The title *Science* is a registered trademark of AAAS.